# Confirming the Revised C-Terminal Domain of the MscL Crystal Structure

Joshua A. Maurer,*‡ Donald E. Elmore,†‡ Daniel Clayton,§ Li Xiong,† Henry A. Lester,§ and Dennis A. Dougherty‡

*Department of Chemistry, Washington University, St. Louis, Missouri 63130; †Department of Chemistry, Wellesley College, Wellesley, Massachusetts 02482; and ‡Division of Chemistry and Chemical Engineering and §Division of Biology, California Institute of Technology, Pasadena, California 91125

ABSTRACT The structure of the C-terminal domain of the mechanosensitive channel of large conductance (MscL) has generated significant controversy. As a result, several structures have been proposed for this region: the original crystal structure (1MSL) of the *Mycobacterium tuberculosis* homolog (Tb), a model of the *Escherichia coli* homolog, and, most recently, a revised crystal structure of Tb-MscL (2OAR). To understand which of these structures represents a physiological conformation, we measured the impact of mutations to the C-terminal domain on the thermal stability of Tb-MscL using circular dichroism and performed molecular dynamics simulations of the original and the revised crystal structures of Tb-MscL. Our results imply that this region is helical and adopts an $\alpha$-helical bundle conformation similar to that observed in the *E. coli* MscL model and the revised Tb-MscL crystal structure.

## INTRODUCTION

In 1998, our understanding of ion channel structure was revolutionized by the determination of atomic resolution structures for KcsA (1) and the bacterial mechanosensitive channel of large conductance (MscL) (2). These and subsequent structures have made it possible to study ion channel structure-function relations in the context of atomic-level protein maps. However, some details of these structures have been inconsistent with biochemical and electrophysiological data and chemical intuition, including the C-terminal region of the *Mycobacterium tuberculosis* (Tb) MscL crystal structure.

Overall, the original high-resolution crystal structure of Tb-MscL (1MSL) (2) led to exciting new revelations about how mechanosensitive ion channels function. Mechanosensitive ion channels are involved in a wide range of physiological processes, from osmoreglation in bacteria to touch, circulation, and hearing in higher organisms (3). The bacterial mechanosensitive channel of large conductance has proven to be a useful model for mechanosensation since its initial identification and cloning from *Escherichia coli* (4). Because MscL channels are quite amenable to mutagenesis, expression, purification, and electrophysiological characterization in bacterial spheroplasts and lipid vesicles, they have become the best characterized mechanosensitive channels (3,5–7).

The gross structural characteristics of the original Tb-MscL structure have been verified biochemically and electrophysiologically (8–10). In particular, Sukharev, Guy, and co-workers (11–13) were able to use this crystal structure along with experimental cross-linking data to develop detailed molecular gating models for *E. coli* (Ec) MscL. In other studies, Perozo, Martinac, and co-workers (14) were able to develop MscL gating models by interpreting site-directed spin-labeling data in the context of the crystal structure. The presence of a high-resolution structure has also allowed MscL gating to be considered with molecular dynamics (MD) simulations (15–17).

Most of these studies considering MscL gating focused on the transmembrane regions of the channel. One reason for this focus was that initial studies implied that the C-terminal region played no discernable role in Ec-MscL function and that a large portion of this region could be cleaved off without altering channel gating (18,19). However, charged residues at the beginning of this region are clearly important for channel function (20), and even mutations and cleavages to the more distal regions of the protein in the C-terminal region do have some effect on the channel physiology of Ec-MscL (21). As a result, this region of the protein clearly has a significant physiological role, although the details of this role have not been worked out.

The C-terminal region of the original crystal structure (1MSL) adopted a striking helical bundle that placed negatively charged residues pointing toward each other. Early MD simulations from our group suggested that this helical conformation was unstable (22), although subsequent TASP studies implied that this region does, in fact, adopt a primarily $\alpha$-helical conformation (23). Sukharev and co-workers modeled this region of the Ec-MscL homolog as a helical bundle based on MD and cross-linking studies (21), placing charged residues on the outside of the bundle and burying hydrophobic residues on the inside of the bundle. In a recent revision (2OAR) made by Rees and co-workers to the original Tb-MscL crystal structure (24), this region assumed a

*Submitted December 6, 2007, and accepted for publication January 23, 2008.*

Joshua A. Maurer and Donald E. Elmore contributed equally to this work.

Address reprint requests to Joshua A. Maurer, Dept. of Chemistry, Washington University, St. Louis, MO 63130. Tel.: 314-935-4695; E-mail: maurer@wustl.edu; or Donald E. Elmore, Dept. of Chemistry, Wellesley College, Wellesley, MA 02482. Tel.: 781-283-3171; E-mail: delmore@wellesley.edu.

Editor: Eduardo Perozo.



0006-3495/08/06/4662/06 $2.00

doi: 10.1529/biophysj.107.127365

conformation similar to Sukharev's Ec-MscL model. However, it should be noted that Tb-MscL and Ec-MscL show different electrophysiological properties and are in different sequence subfamilies (8,9). Because there has been significant controversy regarding this section of the Tb-MscL structure, we aimed to confirm the revised structure using MD simulations and experimental measurements of thermal stability. Our results confirm that the Tb-MscL C-terminal region adopts a helical structure and that this structure resembles the 2OAR structure and not the 1MSL structure.

## MATERIALS AND METHODS

### MD simulations

In general, MD simulations of the Tb-MscL C-terminal region were set up analogous to our previous simulations of this region (22). Simulations included all residues after $Tyr^{94}$ from all five subunits of either the original (1MSL) (2) or the revised (2OAR) (24) Tb-MscL crystal structures. The N- and C-termimi were uncharged (-$NH_2$ and -COOH) in the simulations, as neither end is the terminus of the physiological structure. All ionizable side chains were charged in the simulations; no histidine residues were present in the Tb-MscL structure. The initial structures were solvated with explicit SPC water (9411 and 12,127 for the original and revised structures, respectively), and $Na^+$ ions were added to neutralize the overall charge on the systems. Because thermal denaturation studies were performed under low-ionic-strength conditions, no additional ions were added. The systems were subjected to 50 steps of steepest-descents minimization before and after the addition of ions.

MD simulations of these minimized systems were performed in GROMACS 3.3.1 (25) using the Gromos 96 43a1 force field (26). After heating to 298 K over 20 ps, simulations were extended to 20 ns at a constant temperature (298 K) and pressure (1 bar). Temperature and isotropic pressure coupling (27) utilized time constants of 0.1 ps and 1.0 ps, respectively. Position restraints were placed on the $C_\alpha$ atoms of the two N-terminal residues of each subunit to represent conformational restrictions imposed by the overall assembly of the channel. Simulations utilized a 2-fs time step with the LINCS routine to constrain bond lengths (28) and SETTLE to constrain water geometries (29). Lennard-Jones and short-range Coulombic interactions were cut off at 1.0 nm, and long-range electrostatics were calculated using the particle-mesh Ewald method (30) with Fourier grid spacing of 0.10 nm and cubic interpolation. Analyses were performed using tools in the GROMACS suite, with properties averaged over the last 5 ns of trajectories. Figures were produced using PyMOL (31).

### Thermal denaturation studies

#### *Plasmids and strains*

As previously described, Tb-MscL was encoded in the pET 19b vector, and protein expression was performed in an MscL null *E. coli* BL21 strain (2,8). The pET 19b vector provides ampicillin resistance, a His-tag for purification, and isopropyl-$\beta$-D-thiogalactopyranoside control over protein expression. Site-directed mutagenesis of Tb-MscL was performed using the QuikChange protocol (Stratagene, La Jolla, CA); all mutants were verified by sequencing and enzymatic digestion.

#### *Protein expression and purification*

Frozen permastocks of Tb-MscL or Tb-MscL mutations were used to inoculate 25 ml of LB medium with 50 $\mu$g/ml ampicillin. The cultures were grown overnight at 37°C with shaking. LB cultures were used to inoculate 500 ml of TB medium with ampicillin. The resulting TB cultures were grown to mid-log phase and then induced with 1 mM isopropyl-$\beta$-D-thiogalactopyranoside. After induction, the cultures were grown for an additional 2 h at 37°C or in some cases for 3 h at 30°C. Bacteria were then pelleted and resuspended in 50 mM Tris, 75 mM NaCl, 1% $\beta$-dodecyl maltoside (DDM), at pH 7.5 (10 ml) with complete protease inhibitor cocktail (Roche, Indianapolis, IN). The suspensions were then probe sonicated ($4 \times 30$ s) and incubated with shaking for 1 h at 37°C. After incubation, the suspensions were pelleted at $45{,}000 \times g$ for 45 min, and the resulting supernatant was passed through a 0.2-$\mu$m filter. All chromatography steps were carried out on a Vision Workstation (Applied Biosystems, Foster City, CA). The clarified supernatant was subjected to two-dimensional chromatography using a POROS metal chelate affinity column (Applied Biosystems) charged with cobalt chloride in the first dimension and a POROS HQ anion-exchange column (Applied Biosystems) in the second dimension. Elution from the metal chelate column was achieved using an imidazole gradient (0.25 mM to 1 M at pH 7.5) with 0.05% DDM, and elution from the HQ column was achieved using a sodium chloride gradient (0 mM to 1 M) in the presence of 10 mM Tris at pH 7.5 and 0.05% DDM. Buffer exchange and desalting were then performed using a HiPrep 26/10 desalting column (Amersham Pharmacia Biotech, Piscataway, NJ) charged with 1 mM phosphate buffer and 0.05% DDM at pH 7.2. Difficulties were encountered when producing L117I and R118Q. These proteins showed extensive proteolysis of the carboxyl-terminal tail that was not observed for other proteins.

#### *Circular dichroism thermal denaturation*

Thermal denaturation was performed using an Aviv 62 DS circular dichroism spectrophotometer (Aviv Instruments, Lakewood, NJ). Purified Tb-MscL protein samples were diluted to approximately identical concentrations in 1 mM phosphate buffer (pH 7.2) for thermal denaturation. Circular dichroism scans (260–195 nm) showed equivalent helical propensities between samples. The denaturation consisted of heating from 25°C to 95°C, stepping every 2.5°C, and allowing the sample to equilibrate at each temperature for 5 min. After equilibration, the ellipticity of samples at 220 nm was measured with the signal averaged over 30 s.

## RESULTS AND DISCUSSION

### The revised Tb-MscL C-terminal region remains stable in MD simulations

We performed 20-ns MD simulations of the original (1MSL) and revised (2OAR) C-terminal regions using GROMACS (Fig. 1). In both simulations, the C-terminal region (starting at $Tyr^{94}$) was solvated in explicit water molecules with $Na^+$ ions to neutralize the charge of the systems. Position restraints were placed on the two N-terminal residues of each subunit to represent restraints from the transmembrane sections in this region.

As seen previously, the original crystal structure C-terminal region rapidly becomes scrambled in the trajectory (Fig. 1 *A*), losing much of its helical character. Over the last 5 ns of the trajectory, this structure had an average $C_\alpha$ RMS deviation of 5.4 Å from the crystal structure for the helical bundle region of the structure (starting at $Pro^{106}$) (Fig. 2). Conversely, the revised C-terminal structure maintained an $\alpha$-helical bundle throughout the simulation (Fig. 1 *B*), with an average $C_\alpha$ RMS deviation of 1.2 Å from the crystal structure for the helical bundle region (Fig. 2). Additionally, the revised structure showed significantly more structural stability after

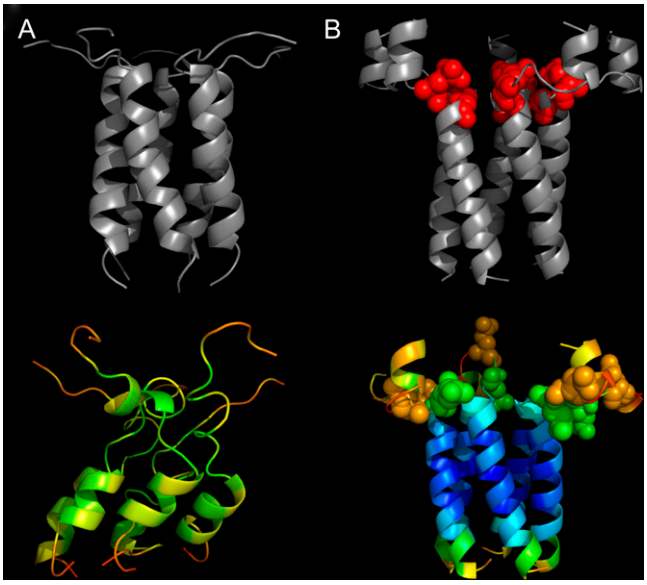


FIGURE 1 Tb-MscL C-terminal region from the original 1MSL (*A*) and revised 2OAR (*B*) structures. Crystal structure conformations are shown on top with 20-ns frames from MD simulations on the bottom. $C_\alpha$ RMS fluctuation values from the last 5 ns of simulations (averaged over all five subunits) are depicted by coloring of the MD structures, with lower fluctuations in cooler (*blue* = 0.5 Å) and higher fluctuations in warmer (*red* = 2.0 Å) colors. $Glu^{102}$ and $Glu^{104}$ are shown in space filling in *B*.

equilibration, with decreased RMS fluctuation in the helical bundle region (Fig. 1).

We used DSSP to further analyze the $\alpha$-helical structure over the course of the simulation and found that the revised structure maintained significantly more helical character than the original structure (Fig. 3). In fact, helicity was rapidly lost in the trajectory of the original structure. Overall, the extent of helicity observed over the last 15 ns of the simulation does not vary significantly for either structure.

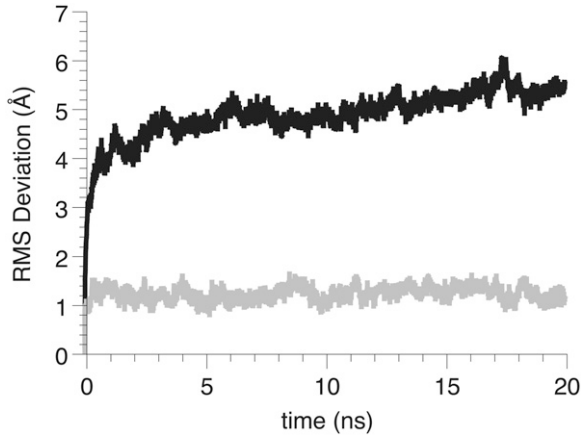


FIGURE 2 $C_\alpha$ RMS deviation from the crystal structure of the helical bundle region in simulations of the original (*solid*) and revised (*shaded*) Tb-MscL structures. Values were calculated for each frame of the simulations by fitting all $C_\alpha$ in the bundle region (defined as starting at $Pro^{106}$) to the crystal structure.

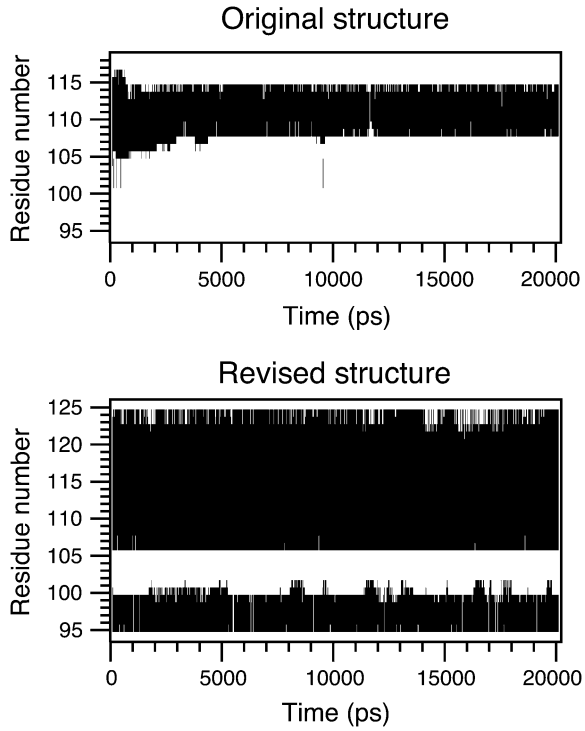


FIGURE 3 DSSP analysis of secondary structure for MD simulations of the original and revised crystal structures. Solid portions on plots represent residues that are $\alpha$-helical at a given point in the trajectories. Results for one representative subunit from each trajectory are shown.

## Thermal stability data are consistent with the revised C-terminal structure

Thermal stability data were collected on several mutants using circular dichroism to verify the revised structure and confirm our simulations. Wild-type and mutant Tb-MscL were expressed and purified as described in the Materials and Methods section, and denaturation as a function of temperature was monitored by the ellipticity at 220 nm. The denaturation curve for wild-type Tb-MscL shows a single melting transition at ~60°C (Fig. 4 *A*). A reduction of 35% in the circular dichroism signal is observed between 25°C and 95°C; relative ellipticity of 0 and 1 are defined at these points in our melting profile. Thus, significant helicity remains in the sample even after the observed transition, which most likely corresponds to the transmembrane domains. After melting, Tb-MscL regains the majority (>90%) of its original ellipticity on returning to 25°C.

We initially compared the thermal stability of several mutants that neutralized acidic residues. The trends for these mutations are consistent with the revised Tb-MscL structure. E102C and E104Q mutations increased stability (Fig. 2 *A*) because these residues are in very close proximity in the revised structure. These acidic side chains strongly repel each other in our MD simulation, leading to a region with very high structural fluctuations (Fig. 1 *B*). Stabilizing this region through neutralizing residue 102 or 104 appears to increase

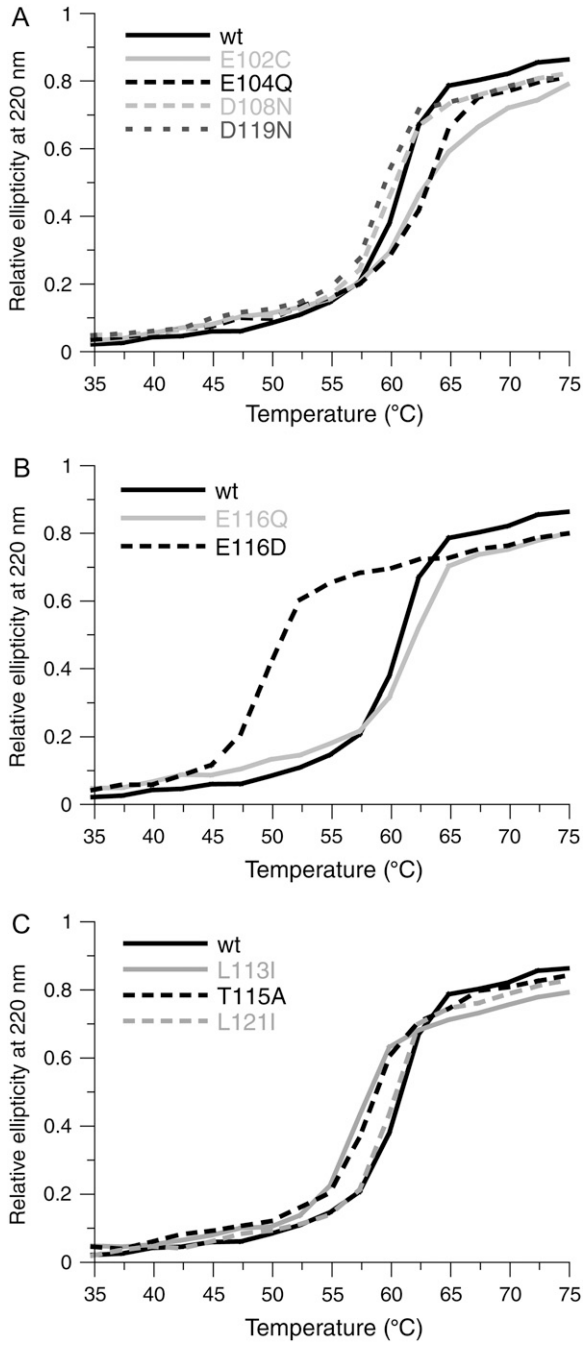


FIGURE 4 Thermal denaturation profiles for a series of single-site C-terminal mutations. In each panel, the denaturation curve for the wild-type channel is shown in black, and mutant channels are shown in dashed and/or shaded lines.

the integrity of the helical bundle in the subsequent region. Interestingly, neutralization of analogous residues dramatically affects gating tension in Ec-MscL (20). Conversely, neither D108N nor D119N mutations significantly altered stability (Fig. 4 *A*), consistent with their relatively isolated positions on the outside of the bundle in the refined structure. Mutations to E116 are discussed in greater detail below.

In our simulation of the revised crystal structure, residues 110–118 exhibited particularly low RMS fluctuations (Fig. 1 *B*). Thus, this region appears to form a ''core'' of the helical structure, and mutations to this core should have a pronounced effect on helical stability. Interestingly, this region includes the highly conserved LLxEIRD motif (residues 113–119) shared throughout the MscL family (21).

Mutations to residue E116 led to particularly intriguing results (Fig. 4 *B*). In the simulation of the revised structure, $Glu^{116}$ is very close to the positively charged $Arg^{118}$ in an adjacent subunit (Fig. 5 *A*). Disrupting this intersubunit interaction clearly could destabilize the helical bundle. In fact, we see that an E116D mutation, which shortens the side chain of residue 116 by one methylene unit, dramatically destabilizes this structure. Clearly, the correct positioning of these residues is critical to the stability of the domain. However, replacement of $Glu^{116}$ with glutamine, an isosteric but uncharged amino acid, actually causes a slight stabilization of this region. At first, it may seem surprising that an E116D mutation dramatically disrupts this interaction whereas E116Q leaves it intact. However, this is consistent with other studies that have shown a hydrogen bond between a charged residue and a good neutral acceptor in a well-solvated region can be as strong as a salt bridge in aqueous solution (32,33).

Two other relatively subtle mutations to this ''core'' region, L113I and T115A, also altered thermal stability (Fig. 4 *C*). Mutation of $Leu^{113}$ to isoleucine results in destabilization of the C-terminal domain. Although, this effect is somewhat surprising for such a conservative mutation, $Leu^{113}$ forms a tight contact with $Leu^{114}$ on the adjacent subunit (Fig. 5 *A*) that apparently is somewhat destabilized by even this slight steric change. The T115A mutation destabilizes the bundle by making the very solvent-exposed side chain of residue 115 significantly more hydrophobic (Fig. 5 *B*). Mutations to I117 and R118 led to extensive proteolysis of the carboxy terminus, which might be a result of destabilization caused by these mutations.

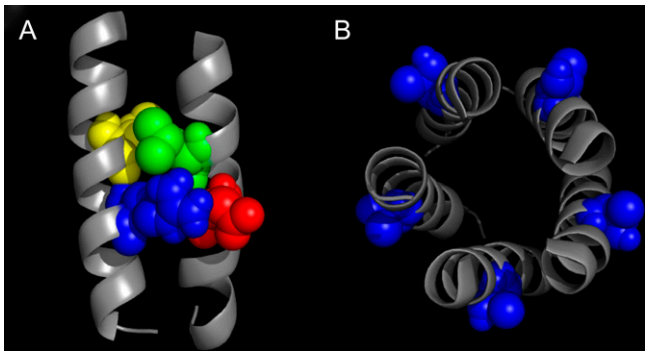


FIGURE 5 Depictions of the final frame from the MD simulation of the revised C-terminal conformation, highlighting (*A*) intersubunit interactions between $Glu^{116}$ (*red*)-$Arg^{118}$ (blue) and $Leu^{113}$ (yellow)-$Leu^{114}$ (*green*), and (*B*) position of $Thr^{115}$ (*blue*). Residues before the helical region are omitted from *B* for clarity.

Conversely, an I121L mutation does not affect thermal stability. Although the $Ile^{121}$ side chain also is involved in hydrophobic packing, it occurs after the ''core'' region of the bundle and has a significantly greater structural fluctuation in the MD trajectory. Thus, subtle changes in its sterics do not appear to have the effect observed for residue 113.

## CONCLUSION

Our computational and experimental results are consistent with the Tb-MscL C-terminal region adopting the revised conformation. This conformation is quite similar to the proposed Ec-MscL model (21). Moreover, our data imply that the helical stability of this bundle is largely dependent on the highly conserved LLxEIRD motif found in almost all MscL sequences as well as in other helical bundles, such as the COMP protein (8,21). Although early studies of MscL suggested little functional relevance for the C-terminal region, more recent work has demonstrated the importance of this region. Intriguingly, the *Synechocystis* sp. and *C. perfringens* homologs, which have nonconserved C-terminal sequences (8), also exhibit distinct electrophysiology from other MscL homologs (34).

As the number of ion channel crystal structures continues to increase, it has become critical to evaluate these structures in light of biochemical evidence. This is especially important because membrane proteins are crystallized in a particularly nonnative environment. Clearly, the original 1MSL structure did not properly define the C-terminal conformation of Tb-MscL, whereas the recently revised 2OAR structure addresses inconsistencies between biochemical and structural data. Similar approaches combining biochemical and computational studies will be useful to confirm ambiguous regions in other channel structures.

This work was partially supported by the National Institutes of Health Program Project Grant GM-62532. Additional support was provided by the Office of the Dean at Wellesley College.

## REFERENCES

1. Doyle, D. A., J. Morais Cabral, R. A. Pfuetzner, A. Kuo, J. M. Gulbis, S. L. Cohen, B. T. Chait, and R. Mackinnon. 1998. The structure of the potassium channel: molecular basis of $K^+$ conduction and selectivity. *Science*. 280:69–77.
2. Chang, G., R. H. Spencer, A. T. Lee, M. T. Barclay, and D. C. Rees. 1998. Structure of the MscL homolog from *Mycobacterium tuberculosis*: a gated mechanosensitive ion channel. *Science*. 282:2220–2226.
3. Hamill, O. P., and B. Martinac. 2001. Molecular basis of mechanotransduction in living cells. *Physiol. Rev.* 81:685–740.
4. Sukharev, S. I., P. Blount, B. Martinac, F. R. Blattner, and C. Kung. 1994. A large-conductance mechanosensitive channel in *E. coli* encoded by MscL alone. *Nature*. 368:265–268.
5. Maurer, J. A., and D. A. Dougherty. 2003. Generation and evaluation of a large mutational library from the *Escherichia coli* mechanosensitive channel of large conductance, MscL—implications for channel gating and evolutionary design. *J. Biol. Chem.* 278:21076–21082.
6. Sukharev, S., and A. Anishkin. 2004. Mechanosensitive channels: What can we learn from ''simple'' model systems? *Trends Neurosci.* 27:345–351.
7. Sukharev, S. I., P. Blount, B. Martinac, and C. Kung. 1997. Mechanosensitive channels of *Escherichia coli*: the MscL gene, protein, and activities. *Annu. Rev. Physiol.* 59:633–657.
8. Maurer, J. A., D. E. Elmore, H. A. Lester, and D. A. Dougherty. 2000. Comparing and contrasting *Escherichia coli* and *Mycobacterium tuberculosis* mechanosensitive channels (MscL). New gain of function mutations in the loop region. *J. Biol. Chem.* 275:22238–22244.
9. Moe, P. C., G. Levin, and P. Blount. 2000. Correlating a protein structure with function of a bacterial mechanosensitive channel. *J. Biol. Chem.* 275:31121–31127.
10. Sukharev, S. I., M. J. Schroeder, and D. R. Mccaslin. 1999. Stoichiometry of the large conductance bacterial mechanosensitive channel of *E. coli*. A biochemical study. *J. Membr. Biol.* 171:183–193.
11. Betanzos, M., C. S. Chiang, H. R. Guy, and S. Sukharev. 2002. A large iris-like expansion of a mechanosensitive channel protein induced by membrane tension. *Nat. Struct. Biol.* 9:704–710.
12. Sukharev, S., M. Betanzos, C. S. Chiang, and H. R. Guy. 2001. The gating mechanism of the large mechanosensitive channel MscL. *Nature*. 409:720–724.
13. Sukharev, S., S. R. Durell, and H. R. Guy. 2001. Structural models of the MscL gating mechanism. *Biophys. J.* 81:917–936.
14. Perozo, E., D. M. Cortes, P. Sompornpisut, A. Kloda, and B. Martinac. 2002. Open channel structure of MscL and the gating mechanism of mechanosensitive channels. *Nature*. 418:942–948.
15. Colombo, G., S. J. Marrink, and A. E. Mark. 2003. Simulation of MscL gating in a bilayer under stress. *Biophys. J.* 84:2331–2337.
16. Gullingsrud, J., and K. Schulten. 2003. Gating of MscL studied by steered molecular dynamics. *Biophys. J.* 85:2087–2099.
17. Kong, Y., Y. Shen, T. E. Warth, and J. Ma. 2002. Conformational pathways in the gating of *Escherichia coli* mechanosensitive channel. *Proc. Natl. Acad. Sci. USA*. 99:5999–6004.
18. Blount, P., S. I. Sukharev, M. J. Schroeder, S. K. Nagle, and C. Kung. 1996. Single residue substitutions that change the gating properties of a mechanosensitive channel in *Escherichia coli*. *Proc. Natl. Acad. Sci. USA*. 93:11652–11657.
19. Hase, C. C., A. C. Le Dain, and B. Martinac. 1997. Molecular dissection of the large mechanosensitive ion channel (MscL) of *E. coli*: mutants with altered channel gating and pressure sensitivity. *J. Membr. Biol.* 157:17–25.
20. Kloda, A., A. Ghazi, and B. Martinac. 2006. C-terminal charged cluster of MscL, RKKEE, functions as a pH sensor. *Biophys. J.* 90:1992–1998.
21. Anishkin, A., V. Gendel, N. A. Sharifi, C. S. Chiang, L. Shirinian, H. R. Guy, and S. Sukharev. 2003. On the conformation of the COOH-terminal domain of the large mechanosensitive channel MscL. *J. Gen. Physiol.* 121:227–244.
22. Elmore, D. E., and D. A. Dougherty. 2001. Molecular dynamics simulations of wild-type and mutant forms of the *Mycobacterium tuberculosis* MscL channel. *Biophys. J.* 81:1345–1359.
23. Kochendoerfer, G. G., J. M. Tack, and S. Cressman. 2002. Total chemical synthesis of a 27 kDa TASP protein derived from the MscL ion channel of *M. tuberculosis* by ketoxime-forming ligation. *Bioconjug. Chem.* 13:474–480.
24. Steinbacher, S., R. Bass, P. Strop, and D. C. Rees. 2007. Structures of the prokaryotic mechanosensitive channels MscL and MscS. *Curr. Top. Membr.* 58:1–24.
25. Van Der Spoel, D., E. Lindahl, B. Hess, G. Groenhof, A. E. Mark, and H. J. C. Berendsen. 2005. GROMACS: Fast, flexible, and free. *J. Comput. Chem.* 26:1701–1718.
26. Van Gunsteren, W. F., S. R. Billeter, A. A. Eising, P. H. Hünenberger, P. Krüger, A. E. Mark, W. R. P. Scott, and I. G. Tironi. 1996. Biomolecular Simulation: The GROMOS96 Manual and User Guide. Hochschulverlag AG an der ETH Zürich, Zürich, Switzerland.

27. Berendsen, H. J. C., J. P. M. Postma, W. F. Van Gunsteren, A. Dinola, and J. R. Haak. 1984. Molecular dynamics with coupling to an external bath. *J. Chem. Phys.* 81:3684–3690.

28. Hess, B., H. Bekker, H. J. C. Berendsen, and J. G. E. M. Fraaije. 1997. LINCS: A linear constraint solver for molecular simulations. *J. Comput. Chem.* 18:1463–1472.

29. Miyamoto, S., and P. A. Kollman. 1992. SETTLE: An analytical version of the SHAKE and RATTLE algorithms for rigid water models. *J. Comput. Chem.* 13:952–962.

30. Darden, T. D., D. York, and L. Pedersen. 1993. Particle mesh Ewald: An N log(N) method for Ewald sums in large systems. *J. Chem. Phys.* 98:10089–10092.

31. Delano, W. L. 2002. The PyMOL Molecular Graphics System. DeLano Scientific, Palo Alto, CA.

32. Hendsch, Z. S., and B. Tidor. 1994. Do salt bridges stabilize proteins? A continuum electrostatic analysis. *Protein Sci.* 3:211–226.

33. Sun, D. P., U. Sauer, H. Nicholson, and B. W. Matthews. 1991. Contributions of engineered surface salt bridges to the stability of T4 lysozyme determined by directed mutagenesis. *Biochemistry.* 30:7142–7153.

34. Moe, P. C., P. Blount, and C. Kung. 1998. Functional and structural conservation in the mechanosensitive channel MscL implicates elements crucial for mechanosensation. *Mol. Microbiol.* 28: 583–592.